Yaw control-related wind turbine's fatigue loads and power forecasting based on machine learning with the consideration of wake effects in wind farms

Ruiyang He[a, *], Hongxing Yang[a, *], Shilin Sun[b], Lin Lv[a], Haiying Sun[a], Xiaoxia Gao[c]

a Renewable Energy Research Group (RERG), Department of Building Services Engineering, The Hong Kong Polytechnic University, Hong Kong

b Department of Mechanical Engineering, Tsinghua University, Beijing, 100084, China

c Department of Power Engineering, North China Electric Power University (Baoding), China

* Corresponding author

E-mail address: ruiyang.he@connect.polyu.hk; hong-xing.yang@polyu.edu.hk

Abstract

Yaw control is one of the most promising active wake control strategies to maximize the total power generation of wind farms. Meanwhile, structural performance has been shown to need to be considered in yaw optimization. Since most wind turbines (WTs) are sunk into the wake flow of upstream counterparts, the combination of wake effects and yaw adjustment complicates the calculation of structural loads. However, efficient and accurate calculation of fatigue loads associated with yaw operation is essential to the yaw-based optimization. In this study, in order to efficiently evaluate the structural performance of yawed WT under wake effects, five fatigue loads at critical WT components and corresponding power output are predicted by machine learning. To achieved this, various inflow conditions, including both free stream and wake inflow combined with practical yaw control

angles, are selected as inputs to machine learning models. Then support vector regression (SVR) model is trained and estimated to find the optimal surrogate. The superiority of the selected SVR based method is verified by comparing with another algorithm in several metrics. The prediction accuracy under various inflow conditions, yaw angles, and wind speeds are analyzed in details. The results show that the selected features are overall sufficient to predict fatigue loads and power yield of any given WT in farms under yaw control. The proposed fatigue loads and power prediction method is expected to make contributions to the yaw-based multi-objective optimization of a wind farm.

Keywords: *Wind farm; Fatigue loads; Machine learning; Yaw control; Wake flow*

1. Introduction

As carbon neutrality being put on the agenda, renewable energy sources are being deployed on a large scale. In particular, as one of the fastest growing renewable energy, wind energy hits milestone with 82GW new installation in 2020 and is expected to have an annual installation of 180GW in future, as reported by the Global Wind Energy Council (GWEC) [1].

With the boost of wind energy, large wind farms with huge capacities play an important role in providing sustainable green electricity. However, wind turbines (WTs) installed in deep rows of a wind farm are exposed to variable inflow profiles and mechanical loads caused by wake effects from upstream WTs [2]. The wake effects are characterized as higher turbulent level and lower velocity compared with the free stream. More importantly, multi-wake interactions and wind direction changes increase the complexity and imbalance of wake flow, lowering the power generation and exacerbating fatigue loads. Therefore, mitigating the wake effects experienced by downstream WTs is critical for lifetime extension and power output

improvement.

Recently, the techniques of active wake control (AWC) have been proven worth considering [3,4]. Active yaw control (AYC), as one of the most promising AWC methods, is a strategy to intentionally redirect the wake away from the downstream WTs with the purpose of achieving the net power increase in the entire wind farm [5] [3,6]. The superiority of yaw techniques in terms of enhancement in power yield is verified by making comparison with other AWC techniques like tilt and pitch control [7] [8]. The performance of yaw misalignment was investigated experimentally through Ref. [6,9–11], of which significant power increase of a wind farm [6][10] and the secondary wake steering [11] were observed. Miao et al. [12] further confirmed the effectiveness of wake steering optimization with positive yaw angles while claiming that negative yaw angles may have adverse effects. The authors indicated that this phenomenon can be explained as the weaker wake deviation as a result of its reaction with clockwise-rotating blades. Additionally, Simley et al. [13] conducted a comparative study and found that accounting for dynamic variability of wind direction can benefit yaw-based optimization in power improvement. The farther the separation distance, the greater the effectiveness. Similarly, variability and uncertainty of wind direction were considered in the yaw optimization strategies by Rott [14] and Quick [15].

Active yaw control has been proved to be beneficial in terms of the total power yields of wind farms, but some studies [4,5,16] show that improperly designed yaw angle will lead to the increase of fatigue loads. Consequently, when applying yaw optimization to maximize the power generation in a wind farm, it is essential to take the corresponding mechanical loads into account in case the adverse structural performance offsets the benefit of yaw-based power increase.

In order to predict the yaw control-related fatigue loads of WTs in wind farms, the fatigue characteristics of WT in yaw conditions and the factors affecting them need to be clarified. Studies[17,18] have found that damage equivalent load (DEL) of blade root edgewise moment is mainly influenced by gravitational loads, therefore,

being almost flat with the variation of yaw angles. However, the equivalent flapwise moment at blade root is highly related to unstable wind loads and therefore the yaw angles. In particular, the DEL of flapwise moments show asymmetric around the unyawed baseline, of which positive yaw angles result in lower DEL while negative yaw angles lead to higher DEL [7,19]. The mainstream explanation [20–23] is that that is attributed to wind shear since it counteracts the advancing and retreating effect of blades for positive misalignment, resulting in the lowest loads at some positive yaw angles. Accordingly, Ennis et al. [21] suggested that wind shear should be taken into account in the wind turbine yaw optimization controller. As for the effect of turbulence intensity on DEL, Kragh and Hansen [24] revealed that after wind speeds slightly higher than rated, optimal wake steering can be achieved without loss of power, while mitigating fatigue loads on downstream WTs due to the reduction of TI enabled by wake redirection .When the TI is low, the flapwise DEL can be significantly influenced by yaw angles. As a result, a maximum of 20% fatigue loads reduction can be achieved at lower TI by yaw but it may be penalized by the load increase of other components of the turbine. Likewise, Kanev et al. [22] concluded that increasing TI makes flapwise DEL less sensitive to yaw angle while its effect on tower bottom needs further investigation.

Although the existing models with sufficient resolution are able to capture dynamic structural performance from wind conditions [3,25], they are computationally expensive and therefore not suitable for applications requiring quick responses and many assessments, particularly yaw-based optimization. Besides, as a rudimentary forecasting methods, lookup table (LUT) [23] seems to be insufficient to provide accurate results. In this case, machine learning-based method can become a favorable surrogate to predict fatigue loads of wind turbines with both high accuracy and efficiency. With data stemming from SCADA measurements, Obdam [26] trained a neural network (NN) model to estimate the tower bottom loads of an offshore WT. Cosack et al. [27] tested the prediction performance of four load estimation procedures, including classical regression methods, conventional physical models,

state estimators and NN models. Among them, the statistical parameters of standard signals without any extra sensors were mapped to the fatigue loads by a NN model and the results showed relatively small errors. In Ref. [28], flapwise and edgewise blade root moments were forecasted with Levenberg-Marquardt back-propagation NN model, of which seven SCADA signals in 48 intervals of 10-min statistics were adopted to train the model. Barthorpe et al. [29] carried out a stationary fatigue experiment for a 9m CX-100 blade and employed non-linear NN models including the Auto-Associative NN model (AANN) and Radial Basis Function (RBF) networks model to commence failure detection. Besides, tower top oscillations from a powerful aeroelastic simulation tool, OpenFAST, were trained by different Artificial Neural Networks (ANN) to construct an economic-tracking Nonlinear Model Predictive Control (etNMPC) system to reduce the fatigue loads of WT tower [30].

However, the machine learning-based method has rarely been studied before in yaw control-related dynamic responses and power prediction, especially under wake conditions. Fatigue forecasting in previous study concerning yaw control is made using either LUT [23] or steady-state model [31]. On the other hand, data obtained from experiments require costly load measurements and a large effort of post-processing [28]. If the sample size is not big enough, the prediction accuracy cannot be guaranteed. Also, the cup anemometer of SCADA installed on the nacelle can only record one wind speed. As mentioned before, wind shear has a significant effect on flapwise equivalent loads, therefore only one wind speed (usually at hub height) is inadequate to describe the wind profile for free flow, let alone the wake flow and wake superposition.

In this study, yaw control-related fatigue loads and power prediction under wake effects are performed using support vector regression combined with high-fidelity aero-elastic tool. The main contributions of this study are outlined as follows. (1) Typical relative distances between WTs are employed to generate various wake effects in wind farms and almost 60% fatigue forecasting of yawed WT are calculated based on wake inflow conditions. (2) Yaw angles from -30 degrees to 30 degrees are

considered in fatigue loads prediction, making it valuable in building up yaw-based multi-objective optimization control system. (3) Wind shear and turbulent intensity are considered to generate both free stream and wake flow, so that the true responses of components under yaw controls can be reflected. (4) Due to the adaptation of a machine learning algorithm and high-fidelity aero-elastic code, the proposed model is cost-effective and reliable, which is particularly suitable for yaw-based real-time optimization. (5) The wind profile input of the proposed prediction method can be obtained by either numerical model or LiDAR measurements. The easy availability of data ensures the universality and practicability of this model.

The remaining of this paper is organized as follows. In section 2, the modeling approach will be introduced in detail, of which the wind field modeling approaches including both free flow and wake flow are described. The second part of this section shows how the fatigue loads are calculated and then converted into comparable DEL. In section 3, the machine-learning based method for fatigue loads prediction and corresponding scenarios of data preparation are discussed. Then the modelling procedure and evaluation criteria are also introduced. In section 4, the superiority of the fatigue loads and power prediction method is verified and the factors that may affect prediction accuracy are investigated. Finally, key findings and conclusions of this study are drawn and listed. The proposed method is capable of predicting fatigue loads in yawed conditions with high accuracy and efficiency and therefore making contributions to yaw-based multi-objective optimization.

2. Fatigue modeling of WTs in wind farms

In order to predict the turbine fatigue loads and power output through the method of machine learning, a large amount of effective data is needed to build the database. Compared with data from field measurements, wind field modeling can conveniently generate a large dataset for training uses. Besides, all possible inflow conditions can be taken into account through modeling, making the database diverse enough to predict the fatigue loads under yaw control of any given WT in farms. In this study,

thousands of fatigue load modeling are carried out first through a method that strikes a balance between accuracy and computational efficiency. The NREL 5MW baseline wind turbine (NREL 5MW hereafter) is adopted as the turbine model.

This section presents the method of full-field turbulent wind modeling, including both free flow and wake flow. Furthermore, an aeroelastic method of WT fatigue load calculation for any given inflow condition is introduced. According to the common practice of fatigue estimation, the obtained time-series data is then transferred to damage equivalent loads (DEL) for comparison.

2.1 Wind field modeling

In this study, thousands of realistic time series of wind fields are generated by the TurbSim code, which is a stochastic, full-field and turbulent wind simulator developed by NREL [32]. In TurbSim, by means of inverse Fast Fourier Transform (IFFT), classical turbulent spectral models, such as IECKAI and IECVKM [32], can be used to generate time-series of three-components wind-speed vectors at points in a vertical grid. The height and width of the wind field grid are selected to be 240m and 1084m, respectively, to be large enough to accommodate different layouts of WT pairs. According to the IEC standard [33], 600s continuous operational signals of the fluctuating load are required for DEL calculation. Therefore, the analysis time of TurbSim is set as 800s and only the last 600s are selected for stability. Characteristics of flow field like turbulent intensity, shear exponent and mean velocity at reference height can be specified. Detailed information of parameter selection regarding wind speed, turbulent intensity and shear exponent will be explained in *Section 3.2 Scenarios of dataset preparation*.

With the large-scale exploitation of wind power, wind turbines in a farm are typically sunk into the wake of their upstream counterparts. Therefore, in the far wake region (usually about 5D, D denotes the diameter of WT) where downstream WTs are typically installed, the flow field perceived by these WTs is quite complicated. Compared with the sheared free stream directly generated by TurbSim, the wake flow

behind a WT is always characterized as approximately three-dimensional Gaussian shape with lower wind speed and higher turbulent level [34]. Moreover, the relative distances between WTs are various due to differences in the layout of different wind farms and changes in wind direction. According to the superposition of the wake area and swept area of the downstream rotor, the wake inflow perceived by downstream WT can be categorized into three types: full wake, partial wake and mixing wake.

In this case, an accurate description of wake development and interaction is essential for predicting fatigue loads and power output of WTs in wake flow. Thus, dynamic wake meandering (DWM) in FAST.Farm [35,36], modeling the wake-deficit evolution as a passive tracer with thin shear-layer approximation, is implemented to capture the wake characteristics and therefore derive the effective wind speed perceived by downstream WTs. Furthermore, since the relative distance can be broken down into spanwise spacing and streamwise spacing, these two factors are responsible for generating different layouts of WT pairs. Ultimately, various wake inflow conditions can be generated by the combinations of different relative distances between WTs and free-flow conditions. Detailed information of parameter selection regarding relative distances will be explained in *Section 3.2 Scenarios of dataset preparation*.

2.2 Fatigue loads evaluation

The NREL 5MW WT is selected as the target wind turbine model, which has a diameter of 126m and a hub height of 90m. For detailed specifications of NREL 5MW, please refer to Ref. [37]. The fatigue loads of a wind turbine is calculated by ElastoDyn of OpenFAST [38–40], which serves as a high-fidelity aeroelastic simulator in this study. ElastoDyn adopts the Kane's equation [41] of motion to model a wind turbine structurally and can be stated as:

$$F_r + F_r^* = 0 \tag{1}$$

where F_r and F_r^* are two sets of scalar quantities named genralized active foreces

and generalized inertia forces, respectively. The total generalized active forces compose of the resultant of all applied forces acting on components of a WT, including aerodynamic forces, elastic forces, gravitational forces, generator forces and damping forces:

$$F_r = F_r\big|_{Aero} + F_r\big|_{Elastic} + F_r\big|_{Grav} + F_r\big|_{Generator} + F_r\big|_{Damp} \tag{2}$$

of which,

$$F_r\Big|_{Aero} = \int_0^{R-R_H} {}^{E}v_r{}^{X_i} \cdot F_{Aero}^{S_i} dr_1 \tag{3}$$

where v is the number of particles with mass in the system, ${}^{E}v_r{}^{X_i}$ is the r^{th} partial velocity associated with particle X_i. $F_{Aero}^{S_i}$ is the resultant force of all aerodynamic forces exerting on point S in blade i.

$$F_r\Big|_{Elastic} = \frac{\partial V}{\partial q_r}, \quad V = \frac{1}{2}\sum_{i=1}^{N}\sum_{j=1}^{N} k_{ij} q_i(t) q_j(t) \tag{4}$$

where V is the potential energy and q_r denotes the generalized coordinate. N is the number of degrees of freedom (DOF), k_{ij} is the generalized stiffness, $q_i(t)$ and $q_j(t)$ are the generalized coordinates related to the flexible body.

As for generalized inertia forces, the mass of blades, hub, nacelle and tower contribute to the total inertia forces and can be represented as:

$$F_r^* = F_r^*\big|_B + F_r^*\big|_H + F_r^*\big|_N + F_r^*\big|_T \tag{5}$$

The generalized inertia forces assoicated with blade result from the blade's distribued lineal density $\mu_B(r)$:

$$F_r^*\big|_B = -\int_0^{R-R_H} \mu_B(r)\, {}^{E}v_r{}^{S_i} \cdot {}^{E}a^{S_i} dr_i \tag{6}$$

where ${}^{E}v_r^{S_i}$ is the r^{th} partial velocity associated with point S in blade i and ${}^{E}a^{S_i}$ is the acceleration of the same point in the inertial coordinate.

Similarly, the distributed linear density of the tower, $\mu_T(h)$, contributes to the corresponding generalized inertia forces:

$$F_r^*\big|_T = -\int_0^H \mu_T(h)\,{}^{E}v_r^{T} \cdot {}^{E}a^{T}\,dh \tag{7}$$

where ${}^{E}v_r^{T}$ is the r^{th} partial velocity associated with point T in the tower and ${}^{E}a^{T}$ is the acceleration of the same point in the inertial coordinate.

The generalized inertia forces related with nacelle can be caused by tower deflections, yaw rates and tilt rates:

$$F_r^*\big|_N = {}^{E}v_r^{D} \cdot \left(-m_N\,{}^{E}a^{D}\right) + {}^{E}\omega_r^{N} \cdot \left(-{}^{E}\dot{H}^{D}\right) \tag{8}$$

where ${}^{E}v_r^{D}$ is the r^{th} partial velocity associated with the point D in nacelle, m_N is the mass of nacelle, ${}^{E}a^{D}$ is the acceleration of the center of nacelle mass in the inertial coordinate, ${}^{E}\omega_r^{N}$ is the r^{th} partial angular velocity associated with the nacelle and ${}^{E}\dot{H}^{D}$ is the time derivative of angular momentum of the nacelle about its mass center in the inertia frame.

Similarly, the generalized inertia forces related to hub are:

$$F_r^*\big|_H = {}^{E}v_r^{C} \cdot \left(-m_H\,{}^{E}a^{C}\right) + {}^{E}\omega_r^{H} \cdot \left(-{}^{E}\dot{H}^{C}\right) \tag{9}$$

where ${}^{E}v_r^{C}$ is the r^{th} partial velocity associated with the point C in nacelle, m_H is the mass of nacelle, ${}^{E}a^{C}$ is the acceleration of the center of nacelle mass in the inertial coordinate, ${}^{E}\omega_r^{H}$ is the r^{th} partial angular velocity associated with the

nacelle and ${}^{E}\dot{H}^{C}$ is the time derivative of angular momentum of the nacelle about its mass center in the inertia frame.

For wind turbines experiencing free streams, the full-field turbulent wind vectors generated by TurbSim are adopted by the FAST simulator to calculate the dynamic structural responses. Due to the fatigue fractures usually happening in the alternating shear stress parts, five fatigue loads at critical components of WT are selected as the representatives: flapwise and edgewise bending moment of blade root, yaw moment of yaw bearing as well as fore-after and side-to-side moment of the tower base. Besides that, the power yield under corresponding inflow condition is also selected as an indicator.

It is worth noting that the DOF of first and second blade flapwise modes, fore-aft tower bending modes and side-to-side tower bending modes, the DOF of first edgewise blade mode and the DOF of drivetrain rotational flexibility and generator are enabled. For WTs sunk into the wake flow of upstream WTs, multiple wind turbine combinations are needed to generate various wake flow for the uses of fatigue loads calculation. In this case, simulations are carried out in FAST.Farm [40,42], which calculates the dynamic structural loads (using OpenFAST) of given WTs in a plant using DWM model to account for wake development and interaction.

By applying rainflow cycle-counting algorithm [43], a 10-min (as suggested by IEC standard [33]) continuous operational signals of fluctuating load can be then converted to damage equivalent load, giving the same fatigue damage as the real turbulent flow. The cycles are characterized by ranges with load-mean and an assumption of linear accumulation of load cycles known as Miner's rule [44] is adopted. As denoted by Eq. (1):

$$D = \sum_i \frac{n_i}{N_i\left(L_i^{RF}\right)} \tag{10}$$

where D denotes the total damage, N_i is the number of cycles to failure, n_i is the

cycle count, and L_i^{RF} is the cycle's load range about a fixed value of the mean load. The relationship between load range and cycles to failure can be reflected as follow through the S-N curve [45]:

$$N_i = \left(\frac{L^{ult} - \left| L^{MF} \right|}{\left(\frac{1}{2} L_i^{RF} \right)} \right)^m \tag{11}$$

where L^{ult} is the ultimate design load of the component under consideration, L^{MF} is the fixed load mean and m is the Wöhler exponent, which depends on the material of the specific components of turbines. According to the IEC standard [33], for steel m is 4 and for glass fiber m is approximately 8 to 12. Therefore, the Wöhler exponent for tower and yaw bearing is 4 and that for the blade is 10.

The actual load cycles occur over a spectrum of the load means instead of a fixed mean load assumed in the above equations. Consequently, the Goodman correction model [45] is applied to adjust the load ranges of fatigue cycles, L_i^{RF}, to treat the data as if each cycle occurred about a fixed mean load.

$$L_i^{RF} = L_i^R \left(\frac{L^{ult} - \left| L^{MF} \right|}{L^{ult} - \left| L_i^M \right|} \right) \tag{12}$$

where L_i^R is the load range of i-th cycle about a load mean of L_i^M.

3. Surrogate modeling

The fatigue modeling method described above is sufficient to evaluate structural responses of a yawed WT, but are computationally expensive, let alone to find the optimal yaw angles for all WTs in a wind plant. Since yaw optimization usually requires fast and reliable evaluation of many loads and corresponding power output, a surrogate model based on the five outputs of fatigue modeling as well as power yield is developed. In this study, support vector regression (SVR) is adopted to predict five

fatigue loads and power output due to its strong generalization ability and structural risk minimization principle, which has been successfully applied in non-linear modeling [46–48]. In the same time, a backpropagation-NN (BPNN) model [49] is also trained to make a comparison. It should also be noted that a convolutional NN (CNN) model is selected for comparison, but not presented as the low accuracy.

3.1 The theory of SVR

SVR, as an extension of support vector machine (SVM), was specifically developed by Drucker et.al [50] for regression. The algorithm determines the trade-off between the fitting error minimization and the smoothness of the estimated function. Given training vectors $x_i \in R^p$, $i = 1,...,n$ and a vector $y \in R^n$, the problem solved by SVR can be written as follows:

$$\min_{\omega,b,\xi,\xi^*} \frac{1}{2}\omega^T\omega + C\sum_{i=1}^{n}(\xi_i + \xi_i^*) \tag{13}$$

with constraints,

$$y_i - \omega^T\phi(x_i) - b \le \varepsilon + \xi_i$$

$$\omega^T\phi(x_i) + b - y_i \le \varepsilon + \xi_i^*$$

$$\xi_i, \xi_i^* \ge 0, i = 1,...,n \tag{14}$$

Prediction of samples who is at least ε away from their true value will be penalized by ξ_i or ξ_i^*, depending on whether their predictions lie below or above the ε tube.

The SVR dual problem can be formulated as:

$$\min_{\alpha,\alpha^*} \frac{1}{2}\left(\alpha - \alpha^*\right)^T Q\left(\alpha - \alpha^*\right) + \varepsilon e^T\left(\alpha + \alpha^*\right) - y^T\left(\alpha - \alpha^*\right) \tag{15}$$

with constraints,

$$e^T\left(\alpha-\alpha^*\right)=0$$

$$0\le\alpha_i,\alpha_i^*\le C,i=1,...,n \tag{16}$$

where e is the vector of all ones, Q is an n by n positive semidefinite matrix, $Q_{ij}\equiv K(x_i,x_j)=\phi(x_i)^T\phi(x_j)$ is the kernel. The training vectors are implicitly mapped into a higher dimensional space by the function ϕ.

The prediction is:

$$y=f\left(x\right)=\sum_{i\in SV}(\alpha_i-\alpha_i^*)K(x_i,x)+b \tag{17}$$

where $K(x_i,x)$ is the kernel function. In this study, the non-linear radial basis function (RBF) kernel is adopted and written as:

$$K(x_i,x)=\exp(-\gamma\parallel x-x'\parallel^2) \tag{18}$$

where γ is the kernel function parameter of the RBF kernel.

3.2 Scenarios of dataset preparation

The aim of this study is to make fatigue loads and power prediction of yawed WTs under wake effects by a machine learning method. Based on the previous study [22,23,51,52], the power loss of WTs with yaw angle exceeding $\pm30°$ would not be compensated by the power increase of downstream WTs. Additionally, yaw angles with same absolute value but opposite directions could exert different structural performance on WT due to wind shear [20–23]. Therefore, yaw angles are set as $0°$, $\pm5°$, $\pm10°$, $\pm15°$, $\pm20°$, $\pm25°$, $\pm30°$, of which $-5°$ is neglected considering its low improvement in power output but negative effects on structural performance.

According to the specification of NREL 5MW [37], the cut-in and cut-out speeds of which are 3m/s and 25m/s, respectively. Thus, the inflow speeds are set from 3m/s to 25m/s with an interval of 2m/s. Besides, based on the turbulent intensity observed

in wind farms [49], it is reasonable to set TI from 2% to 26% with an interval of 3%.

For yawed cases under free streams (as the existing research did), the inflow profile would be sheared flow and can be determined by power law as follow.

$$U_0(z) = u_0(\frac{z}{z_0})^{\alpha} \tag{19}$$

where z_0 is the reference height and u_0 is the corresponding wind speed. Here the hub height is set as reference height and therefore the u_0 is the wind speed at hub height. α is the power exponent of the sheared flow, whose range is set from 0.1 to 0.26 with an interval of 0.04.

For yawed cases in the downstream of other WTs, the wake interaction and partial wake will disturb the originally ideal sheared inflow and cause added turbulence intensity. Despite different original wind speed and TI, the factor that effects wake inflows is the relative distance between WTs, which can be broken down into streamwise and spanwise distances (as shown in Fig.1). In terms of streamwise distance, 4D to 7D (D equals 90m for NREL 5MW) with an interval of 1D are adopted due to the typical distance of downstream WTs. For similar reasons, spanwise distances are set as 0D, ±0.5D, ±0.75D, ±1D, ±1.3D.

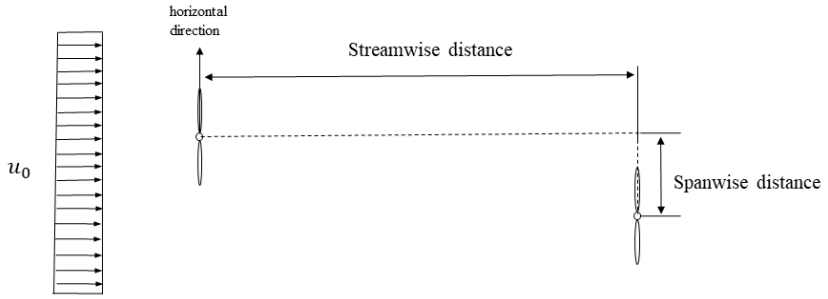

Fig.1 The illustration of streamwise and spanwise distances.

Consequently, it can be concluded that only one speed at hub height (usually obtained by SCADA) is insufficient to describe the inflow profiles of WTs under wake effects. To unify the input variables of cases under different inflow conditions,

in this study, the initial wind speed at hub height, the shear exponent of free flow and streamwise and spanwise spacings that affect wake flow are represented by wind speed of selected nine points (three by three) at rotor plane (as demonstrated in Fig.2) and turbulent intensity at hub height. It should be noted that in addition to being obtained through TurbSim used in this study, the wind speeds of the nine points and TI as input variables can also be obtained through the analytical wake models or LiDAR measurements, giving the proposed fatigue loads and power prediction method great universality and practicability.

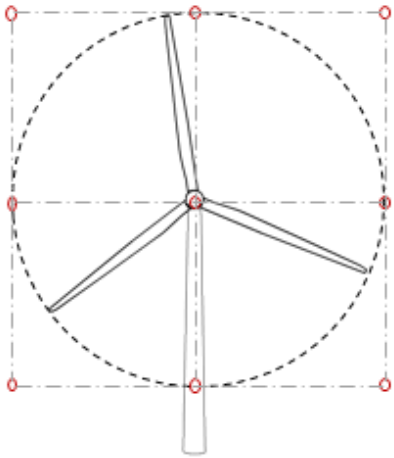

Fig.2 The selected nine points representing wind profile on rotor plane.

To systematically evaluate the structural performance of yawed WTs in wind farms, five fatigue loads are extracted as representatives. In addition to the DEL of flapwise and edgewise loads at blade root that are often employed in existing researches, the DEL of yaw bearing and side-to-side and fore-after tower base are also considered to preserve the possibility for future multi-objective optimization regarding wind farms. Finally, the 10-min averaged electrical power yield under corresponding inflow conditions is added as the sixth output variable of the database.

By skipping redundancy and unnecessary cases, a total of 12728 10-min simulations are carried out to build up the database, including 5600 samples related to free flow and the rest of them to wake flow. Please note that two WTs with such numerous combinations of layouts and inflow conditions are capable of covering the

main situations of wake superposition, therefore being sufficient to build up the database for the purpose of fatigue loads prediction.

3.3 The SVR modeling procedure

In the light of the above Eq. (13) ~ (18) and theory introduced in *3.1 The theory of SVR*, a surrogate method using SVR for fatigue loads and power prediction is developed. The modeling process in this study can be divided into the following steps:

(1). Build up the database and clarify the features and targets. In this study, 12728 samples are prepared, including various free stream (5600 cases) and wake flow (7128 cases) conditions. 11 input variables are composed of 9 points (three by three) of 10-min averaged wind speed at rotor plane, turbulent intensity and yaw angle while 6 outputs are 5 representative fatigue loads of the target wind turbine and its power generation.

(2). Randomly split the dataset into the training set and test set. In this study, the test set is 20% of the whole dataset.

(3). Standardize the dimension features. Standardization of datasets is a common practice for machine learning to avoid large magnitude differences between different dimension features.

(4). Tune the hyper-parameters of SVR. Hyperparameters are parameters that cannot be directly learned from machine learning models. When training an SVR with RBF kernel, the hyperparameters are the coefficient of kernel, C, and the regularization constant, gamma. The grid search method is responsible for exhaustive searching, of which the specified values of C are 1e1,1e2,1e3,1e4, 1e5, 1e6, 1e7, 1e8, 1e9, 1e10 and the specified values of gamma are ranged from -10 to -1 with an interval of 1 spaced evenly on a log scale. The classical five-fold cross-validation [53] is employed to find the optimal hyperparameters.

(5). Train the SVR model with the tuned optimal parameters, make predictions and evaluate the results. The detailed evaluation criteria for targets are explained in

the next section.

3.4 Evaluation criteria for fatigue and power predictions

The performance of the optimized machine learning models can be evaluated using three metrics: normalized root mean square error (NRMSE), mean absolute percentage error (MAPE) and coefficient of regression (R^2).

$$NRMSE(y,\hat{y}) = \frac{\sqrt{\frac{1}{n}\sum_{i=1}^{n}\left(y_i-\hat{y}_i\right)^2}}{y_{\max}-y_{\min}} \tag{20}$$

$$MAPE(y,\hat{y}) = \frac{1}{n}\sum_{i=1}^{n}\frac{\left|y_i-\hat{y}_i\right|}{\max\left(\varepsilon,\left|y_i\right|\right)} \tag{21}$$

$$R^2(y,\hat{y}) = 1-\frac{\sum_{i=1}^{n}\left(y_i-\hat{y}_i\right)^2}{\sum_{i=1}^{n}\left(y_i-\bar{y}\right)^2},\quad \bar{y}=\frac{1}{n}\sum_{i=1}^{n}y_i \tag{22}$$

where y_i is the true value of i-th sample for validation and $\hat{y}_i$ is the corresponding predicted value. $y_{\max}$ and $y_{\min}$ is the maximal and minimal value in n samples of actual output set, respectively. ε denotes an arbitrarily small but positive number in case of undefined results when y is zero while $\bar{y}$ means the average value of actual output.

Note that while the root mean square error (RMSE) is always adopted as an important indicator to reflect the deviation between predicted and true values, its value can be largely influenced by data range. To make comparisons between datasets and models with different scales, the normalized root mean square error (NRMSE) is employed instead by dividing the RMSE by the difference between the maximum and minimum y values. MAPE is a measure of prediction accuracy of forecasting models by linearly averaging all absolute percentage errors. R^2 represents the proportion of the variation of actual value that can be explained by the predicted value, so as to judge the interpretability of the regression models.

4. Results and discussion

4.1 Comparison and validation of the proposed forecasting method

As the machine-learning algorithm of the proposed method for fatigue and power forecasting, the support vector regression method with the best performance (coefficient of kernel is determined to be 0.1 and the regularization constant is 100000) is employed in this section to verify its regression ability. Meanwhile, as a common practice in machine learning, the back-propagation neural network (BPNN) mentioned above is also tuned for comparison. By using the same database as SVR, the best hyperparameters, such as the number of layers and the number of neurons in each layer are determined by means of grid search and cross-validation. The optimal number for the hidden layer of BPNN is turned out to be 2 with 150 neurons in the first layers and 100 neurons in the second layer.

The prediction errors of both ML methods are first listed in Table 1 for comparison. The coefficient of regression R^2 of both methods are relatively high, especially for the prediction of DEL of flapwise and yaw moment, tower-base loads as well as electrical power. However, R^2 of edgewise load of BPNN is smaller than that of SVR. As for MAPE, is most representatives' prediction, these values of BPNN are about two or three times larger than that of SVR. The MAPE of SVR predicted results are almost within 3.5% except for the DEL of side-to-side moment at tower base, which can be attributed to the scenario of wind speed selection. In this study the selected nine points of wind speed cover the whole rotor area, whereas the wind speed that exerts effects on tower base is actually not included for the sake of simplicity. Even though, the predicted results also better match the true value with acceptable precision. The MAPE of power prediction from SVR is still very small, but that from BPNN is rather noticeable. Combined with the corresponding high performance of R^2, this phenomenon can be caused by the relatively low performance in small power forecasting because in this region the ratio of error to true value will be large. This in turn can illustrate that the SVR model is able to provide not only good but also

reliable regression ability in all operating ranges of the wind turbine. Since the root mean square error tends to penalize bias more than linearly averaged relative error such as MAPE, it is an ideal indicator for demonstrating how the predicted value deviates from the true value. It can be noticed that the standard deviation of SVR predicted results is smaller than the counterpart in all targets. In particular, the NRMSE of DEL of edgewise and yawing moment as well as power forecasting are an order of magnitude smaller than that of BPNN, confirming the regression stability of the SVR-based prediction method.

Table 1 Prediction performance comparison for SVR and BPNN.

ML methods	SVR			BP-NN		
	R^2 [-]	MAPE[-]	NRMSE[-]	R^2 [-]	MAPE[-]	NRMSE[-]
$DEL_{Edgewise}$	0.9963	0.4%	0.0082	0.9814	1.0%	0.0169
$DEL_{Flapwise}$	0.9963	3.3%	0.0104	0.9926	5.3%	0.0140
DEL_{Yawing}	0.9996	1.5%	0.0037	0.9971	5.2%	0.0104
$DEL_{\text{Side-to-side}}$	0.9820	7.4%	0.0222	0.9799	9.0%	0.0229
$DEL_{\text{Fore-aft}}$	0.9969	2.9%	0.0100	0.9964	3.9%	0.0113
Power	0.9995	0.7%	0.0082	0.9981	13.0%	0.0184

Corresponding to the MAPE in Table 1, Fig.3 displays the probability density function of relative errors for both ML-based methods. It can be noticed that the overall relative errors of edge moment are an order of magnitude smaller than that of other indicators, of which the majority of SVR errors fall within 0.02% whereas that of BNPP errors are ranged in 0.04%. Additionally, over 30% of SVR predicted results have nearly zero error while the corresponding error probability density of BNPP is

only about 15%. In Fig.3 (b), the probability density of both ML methods has a similar trend, while the SVR predicted errors are smaller compared with the BNPP results with similar density. The margin of SVR errors is also smaller on both sides, indicating a lower probability to make regression with large gaps. In Fig.3 (c), two almost zero error probability densities of SVR together account for more than 70% and as the error increase, the frequency decreases rapidly. On the other hand, the largest error of BPNN is about two or three times larger than that of SVR error. In Fig.3 (d), SVR performances slightly better than the counterpart although the trend of frequency is similar for both methods. The detailed analysis based on different inflow conditions and yaw angles will be presented in the following part of this paper to figure out the potential factors that may influence the accuracy of regression. In Fig.3 (e), although the wind speed that affects fore-after moment is not included in the database as well, the regression ability shown in this figure is much better than the DEL of side-to-side moment. In Fig.3 (f), the difference in probability density is rather huge. Almost all SVR predicted power yields match the true value very well, whereas some relatively large errors occur in the BNPP results. As explained above, prediction gaps in low power regions may largely affect the final performance of BPNN.

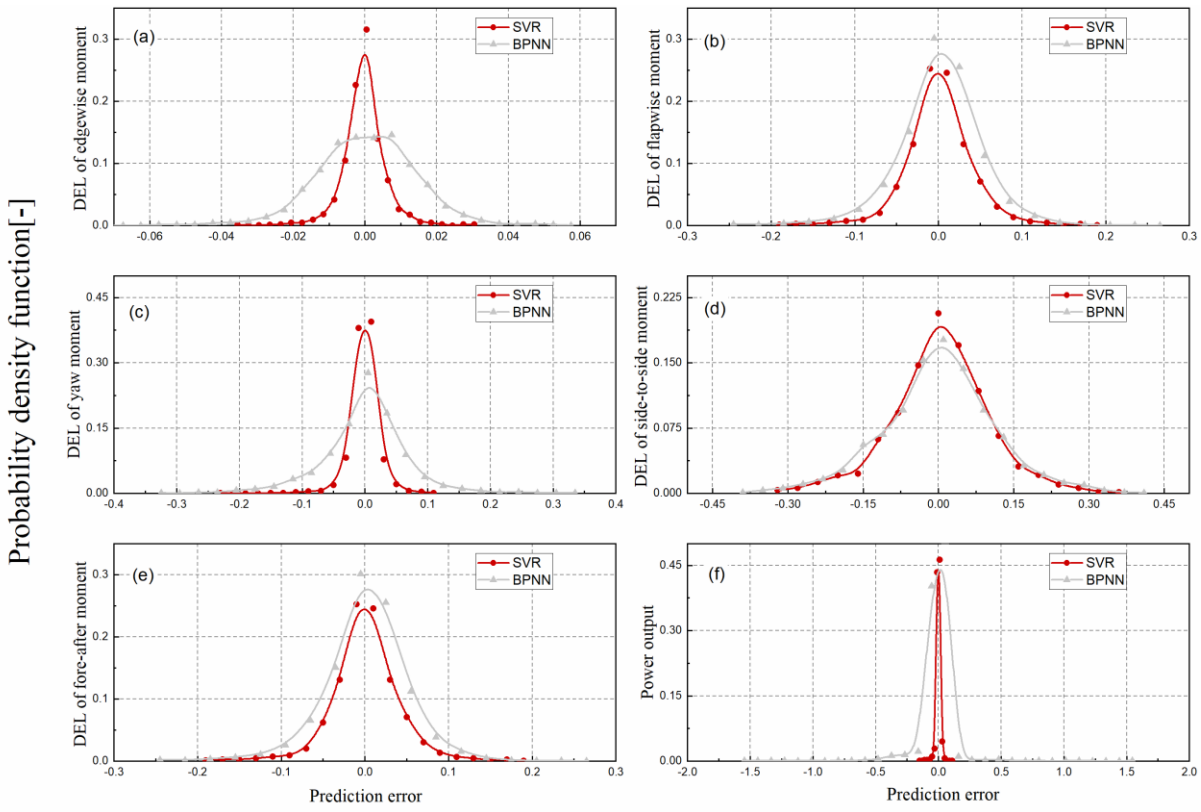

Fig.3 Probability density function of prediction error for fatigue loads and power output of SVR and BPNN.

Fig.4 demonstrates the regression capability of the adopted SVR model for all six targets. It can be concluded that the overall regressions are rather good, returning high R^2 scores for fatigue loads from blade to tower base as well as power prediction. Fatigue loads at blade root in both directions are well forecasted within the whole spread of actual data. Since the variance of DEL of flapwise moment can be substantially affected by yaw angles while that of edgewise moment is dominated by gravitational load, the prediction results verify the rationality of feature selections. More notably, the predictions of fatigue load of the yaw bearing perfectly follow the true values. As for fatigue loads at the tower base, the values in both directions are concentrated below 20000 kN-m. The regression performance of side-to-side fatigue load at larger values is prone to be less accurate than that at lower values while the predictions of fore-after fatigue load work perform well in all fatigue ranges. Therefore, it is safe to say that the regression results of fatigue loads at the tower base are relatively high and acceptable. The predictions of power output are exceedingly

accurate below 2500kw. On the other hand, the predicted values are slightly overestimated above half of the rated power and are underestimated a little when approaching the rated 5000kw. To sum up, the regressions of main representatives of wind turbine performance, including fatigue loads from blade root to tower base and the expected power output, prove that nine points (three by three) of 10-min averaged wind speed at rotor plane combined with TI and yaw angle are sufficient to determine turbine fatigue performance under active yaw controls.

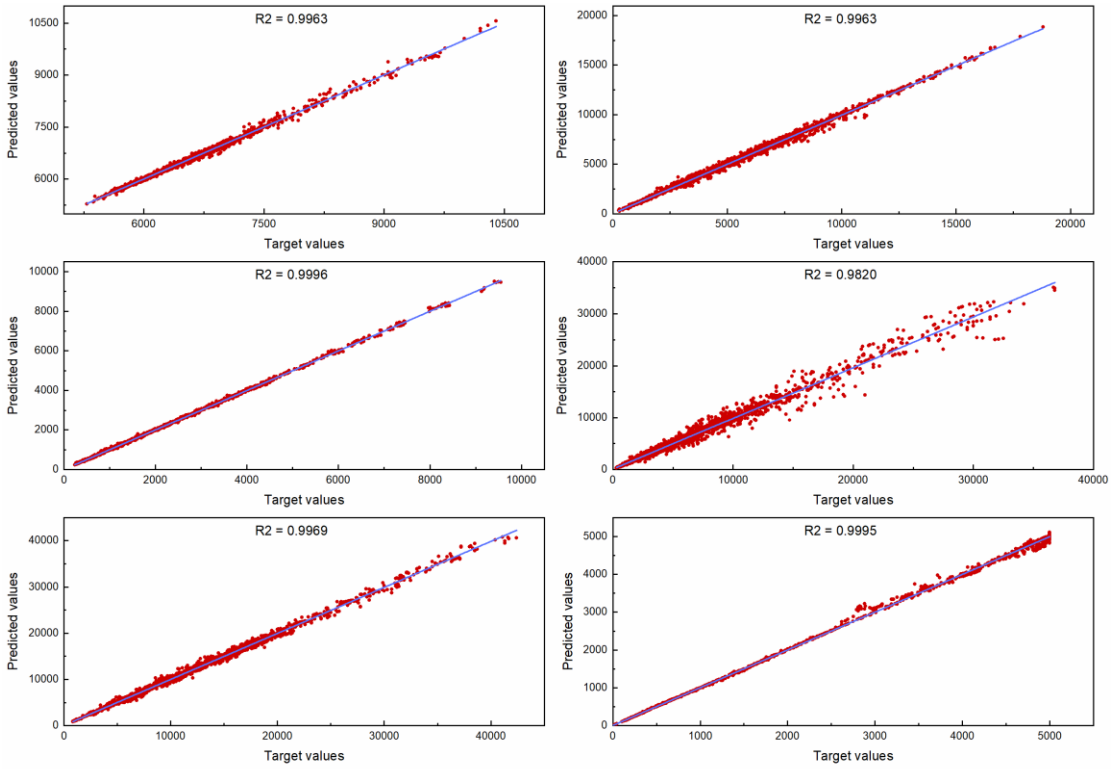

Fig.4 Regression plots of the SVR model. (a) edgewise DEL. (b) flapwise DEL. (c) yaw DEL. (d) side-to-side DEL. (e) fore-after DEL. (f) power output.

Based on the analysis above, it can be concluded that SVR based method outperforms the BPNN based method in terms of fatigue loads and power prediction for yawed turbines in wind farms. The predicted value of SVR can largely determine the true value of all fatigue metrics and power output. The regression ability of SVR is also reflected in smaller mean absolute percentage error as well as higher probability density around zero error or steeper slop as the error value increase. By comparing the root square mean error, the prediction errors of SVR are observed to be

less discrete than that of BPNN, proving its predictive stability for any given yawed WTs in farms.

4.2 Performance analysis

While the superiority of SVR on fatigue loads and power forecasting is verified, the potential factors that affect the prediction accuracy still need to be further investigated. One of the most notable contributions of this work is that the fatigue loads prediction of yawed WTs is not only performed under free stream but also takes the wake inflow into account. Besides, the yaw angles and different wind speed levels may also exert influence on prediction accuracy. Therefore, the factors discussed above are employed to study the performance of proposed fatigue loads and power prediction method in depth.

Fig.5 shows the relative errors of all five fatigue loads and power output under both free stream and wake inflow. It can be seen that except for the side-to-side DEL at the tower base, the prediction precision of all other representatives is as good under the influence of free-flow as under the influence of wake flow, proving that complicated inflow conditions would not harm the accuracy of prediction. The performance of side-to-side moment forecasting is worthy of attention. As we can see the predictions under perturbed wake effects even have better performance than that under sheared inflow. This phenomenon can be explained by the uneven wind distribution in the lateral direction, which is believed to make some contributions to side-to-side moment prediction under yaw conditions compared with fairly uniform distribution under free inflows. Consequently, the complexity of inflow conditions has little effect on the prediction of edgewise, flapwise, yaw and fore-after DEL as well as power yield while the perturbed wake inflow is found to be beneficial of side-to-side DEL prediction.

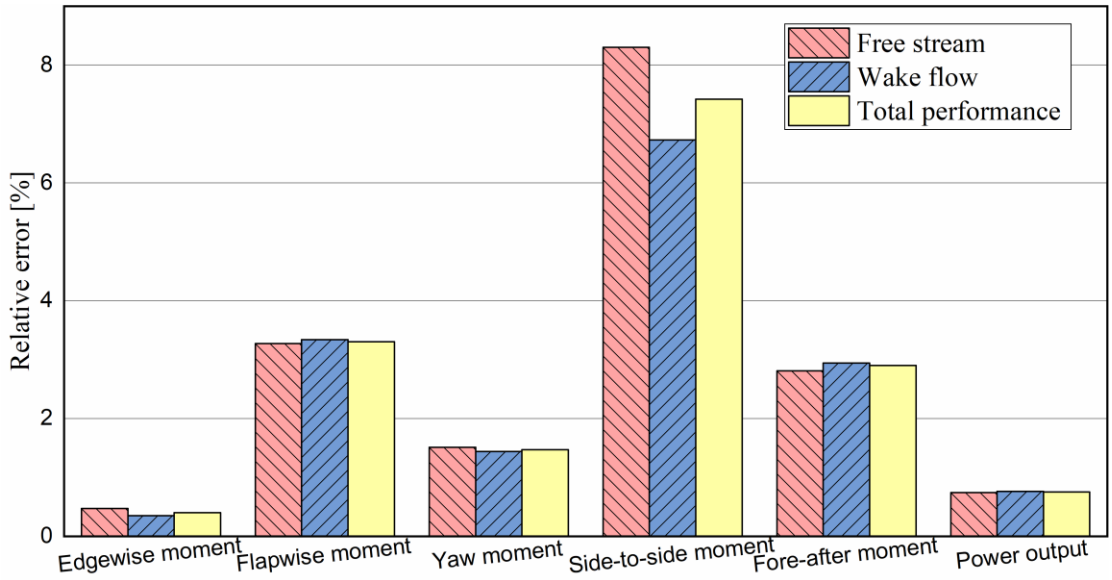

Fig.5 Comparison of prediction accuracy under free stream and wake flow conditions.

Fig.6 illustrates the relative errors of DEL of five representative fatigue loads and power output concerning different yaw angles. It can be seen that the predicted results of edgewise DEL are highly accurate and not affected by the variation of yaw angles. This is due to the fact that it is mainly dominated by gravitational force as explained before. On the other hand, the flapwise moment at blade root can be rather different under different yaw control strategies. Thus, combined with the corresponding error bars shown above can, it can be demonstrated that its accuracy concerning different yaw angles is relatively consistent, except for a minimum value at five degrees. The predicted yaw DEL of yaw bearing also matches the true values very well at different yaw angles, leaving only that of 30 degrees above 2%. It is observed that the side-to-side DEL at tower base has the biggest relative errors at all yaw angles, mainly because the wind speed is chosen for this study only covers the area swept by rotor without considering the wind speed along with the tower. In the meantime, this figure reveals that its prediction accuracy is dominated by the variation of yaw angle. The prediction error reaches its maximal value at unyawed or nearly unyawed conditions and decreases as the absolute yaw angle increase. Since the side-to-side moment starts to become larger when the rotor plane and wind direction are not perpendicular, its value at unyawed conditions is relatively small, making its prediction error easier to be amplified. On the whole, the yaw control in the positive direction could cause more

error compared with a yaw in the negative direction with the same absolute value. On the contrary, the prediction precision of fore-aft moment at tower base is less affected by yaw angle variation, giving the maximal value of no more than 4% at -30 degrees. The yaw angle seems also to have effects on the accuracy of power forecasting, of which bigger yaw angles cause a larger error and small angles generate little error. Although the yaw angles in the negative direction generally produce larger errors than their positive counterparts, the overall power prediction is very precise, with the highest error bar of less than 2%.

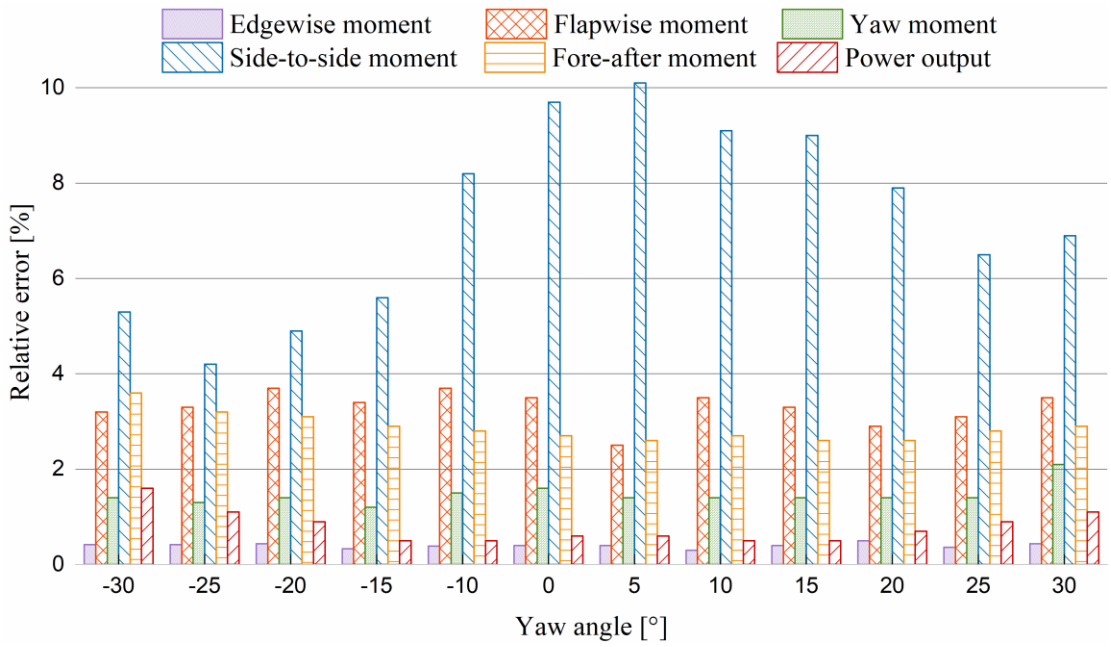

Fig.6 The relative errors of SVR under different yaw angles.

Fig.7 shows the regression accuracy of fatigue loads and power output in terms of different wind speed. It should be noted that the wind speed at hub height is chosen as the representative and the rated wind speed of selected NREL 5MW is 11.4 m/s. The prediction accuracy of edgewise DEL is found to be rarely affected by the wind speed though the maximal error appears around the rated speed. The error of flapwise DEL decreases with the increase of wind speed by and large. The biggest value belongs to the 3~5 m/s group, which could also be explained by a relatively small denominator compared with flapwise DEL under larger inflow wind speed. The performance of SVR on yaw DEL prediction is constantly accurate along with the

wind speed from cut-in to cut-out, giving the biggest one of only 2.2% appeared in the 6~8 m/s group. The obvious large error of side-to-side DEL starts to decrease after 15~17 m/s, which means that the proposed selection of wind speed representative points would be more effective when the inflow wind speed at relatively large. As for the fore-after DEL prediction, the error increases along with the wind speed first and then decreases after reaching its maximal value around the rated speed. The maximal error of power prediction is 1.8%, indicating that the overall performance of SVR on this target is rather accurate. The biggest one appears at 3~5 m/s group, which usually corresponds to little power yield. At this speed group, an error of tens of kilowatts may lead to a notable relative error. However, the relative error itself is very small compared with the BNPP predicted results presented in Table 1. With the increase of wind speed, the accuracy of power forecasting increases comparatively, especially the wind speed after the 11.5~14 m/s group. For unyawed WT under the free stream, the power output can reach its rated value when the wind speed exceeds its rated speed. However, the asymmetric inflow in the lateral direction caused by wake flow and yaw angle can result in power losses to some extent and therefore increase the wind speed at which the rated power yield can be achieved. It is conceivable that both the yaw angle and the perturbed wake inflow conditions have little effect on the power prediction when the speed is large enough. Therefore, it is reasonable that the power prediction error is smaller at high wind speed.

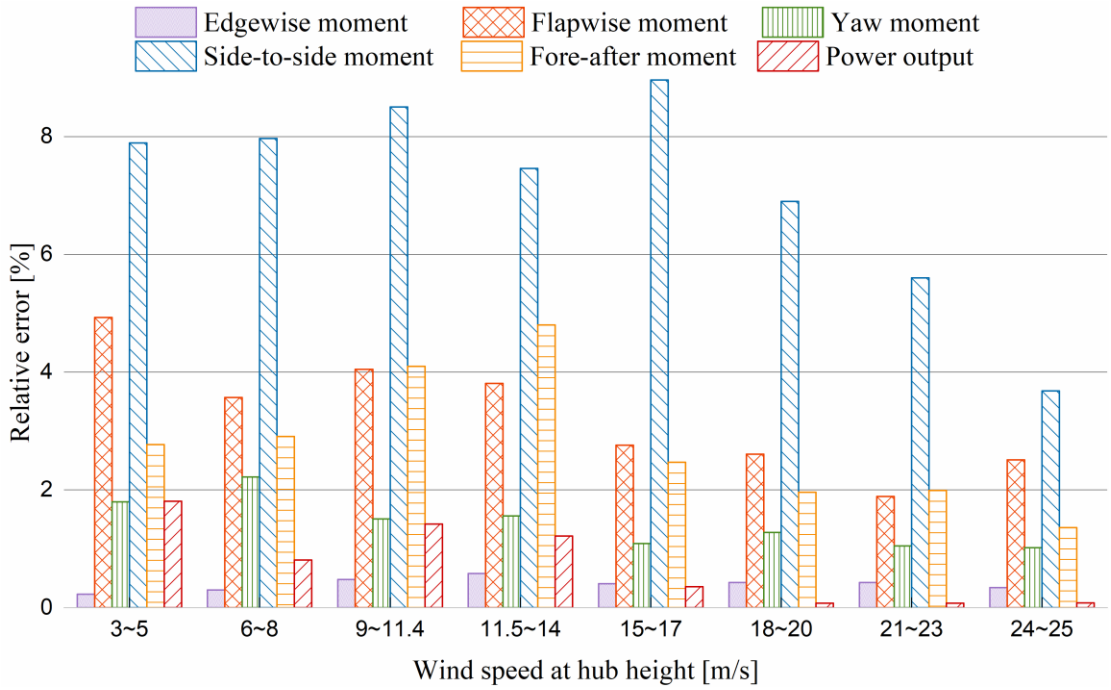

Fig.7 The relative errors of SVR under different wind speed.

5. Conclusion

This study aims to efficiently and accurately predict yaw control-related fatigue loads and power output based on machine learning with the consideration of wake effects in wind farms. The NREL 5MW reference wind turbine is utilized as the turbine model. The TurbSim is adopted to generate realistic free flow and its combination with FAST.Farm is responsible for producing various perturbed wake flows. Fatigue loads at blade root, yaw bearing and tower base where fatigue fractures usually happen as well as corresponding power yield are computed by a high-fidelity aeroelastic code OpenFAST and chosen as the output variables of machine learning. Due to the consideration of wake effects and yaw angles in fatigue loads and power prediction, the proposed method can make contributions to yaw-based multi-objective optimization of wind farms. The main conclusions are drawn and listed as follows.

(1) A comparative study has been performed among different machine learning algorithms to verify the superiority of the proposed prediction approach. The study shows that the accuracy of SVR predicted results of all five fatigue

loads and power output are relatively high and the dispersion of errors is small. Further analysis also indicates that the complicated wake inflow has less effect on prediction accuracy compared with WT perceived free stream. In particular, the asymmetric wake inflow has proven to be beneficial for side-to-side moment forecasting.

(2) Nine points (three by three) of 10-min averaged wind speed covered rotor swept area combined with turbulent intensity and yaw angle are proved to be sufficient to forecast five fatigue loads at critical components and power yield under active yaw controls. Most of the output variables have prediction errors of no more than 3.5%, of which edgewise DEL and power output have even smaller prediction errors, within 1%. Considering the wind speed along the tower is not included, an overall error of 7.4% and a regression coefficient of 0.982 of side-to-side moment at tower base is acceptable.

(3) The accuracy of edgewise and fore-after moments are found to be less affected by the variation of yaw angles. However, the prediction error of side-side moment at tower base seems to strongly depend on yaw angle. Its maximal value is achieved at zero or nearly zero yaw conditions and decreases with the increase of absolute yaw angles. Since the side-to-side DEL is relatively small when the rotor is perpendicular to the wind direction, the denominator of relative error may amplify the prediction gap. Besides, the prediction of side-to-side DEL with negative yaw angles tends to be more accurate than that with positive yaw angles.

(4) The variation of wind speed has proven to have little effect on the prediction of edgewise DEL. However, the prediction error shows an obvious decrease after the 9~11.4m/s wind speed group, indicating that the prediction of this target can be more precise when the inflow wind speed is relatively large. Similarly, the prediction accuracy of power output also increases with the increase of wind speed. Since the yaw angles and disturbing wake inflow can exert little effects on power output when the wind speed is large enough, the prediction gap is small and therefore has a rather high accuracy.

Declaration of Competing Interest

The authors declare that they have no known competing financial interests or personal relationships that could have appeared to influence the work reported in this paper.

Acknowledgment

The work described in this paper was supported by the Research Institute for Sustainable Urban Development (RISUD) with the account number of BBW8 and the FCE Dean Research project with the account number of ZVHL, The Hong Kong Polytechnic University.

References

[1] GWEC. Global Wind Report | Gwec. Glob Wind Energy Counc 2021:75.

[2] Chen Y, Li H, Jin K, Song Q. Wind farm layout optimization using genetic algorithm with different hub height wind turbines. Energy Convers Manag 2013;70:56–65. https://doi.org/10.1016/j.enconman.2013.02.007.

[3] Wingerden JW Van, Ruben SD, Marden JR, Pao LY. Wind plant power optimization through yaw control using a parametric model for wake effects—a CFD simulation study 2016:95–114. https://doi.org/10.1002/we.

[4] Nash R, Nouri R, Vasel-Be-Hagh A. Wind turbine wake control strategies: A review and concept proposal. Energy Convers Manag 2021;245:114581. https://doi.org/10.1016/j.enconman.2021.114581.

[5] Lin M, Porté-Agel F. Power Maximization and Fatigue-Load

Mitigation in a Wind-turbine Array by Active Yaw Control: An les Study. J Phys Conf Ser 2020;1618. https://doi.org/10.1088/1742-6596/1618/4/042036.

[6] Fleming P, Annoni J, Shah JJ, Wang L, Ananthan S, Zhang Z, et al. Field test of wake steering at an offshore wind farm. Wind Energy Sci 2017;2:229–39. https://doi.org/10.5194/wes-2-229-2017.

[7] Fleming PA, Gebraad PMO, Lee S, van Wingerden JW, Johnson K, Churchfield M, et al. Evaluating techniques for redirecting turbine wakes using SOWFA. Renew Energy 2014;70:211–8. https://doi.org/10.1016/j.renene.2014.02.015.

[8] Campagnolo F, Petrović V, Bottasso CL, Croce A. Wind tunnel testing of wake control strategies. Proc Am Control Conf 2016;2016-July:513–8. https://doi.org/10.1109/ACC.2016.7524965.

[9] Bromm M, Rott A, Beck H, Vollmer L, Steinfeld G, Kühn M. Field investigation on the influence of yaw misalignment on the propagation of wind turbine wakes. Wind Energy 2018;21:1011–28. https://doi.org/10.1002/we.2210.

[10] Fleming P, King J, Simley E, Roadman J, Scholbrock A, Murphy P, et al. Initial results from a field campaign of wake steering applied at a commercial wind farm – Part 1. Wind Energy Sci 2020;5:945–58. https://doi.org/10.5194/wes-5-945-2020.

[11] Fleming P, King J, Simley E, Roadman J, Scholbrock A, Murphy P, et al. Continued results from a field campaign of wake steering applied at a commercial wind farm - Part 2. Wind Energy Sci 2020;5:945–58. https://doi.org/10.5194/wes-5-945-2020.

[12] Weipao M, Chun L, Jun Y, Yang Y, Xiaoyun X. Numerical investigation of wake control strategies for maximizing the power generation of wind farm. J Sol Energy Eng Trans ASME 2016;138:1–7.

https://doi.org/10.1115/1.4033110.

[13] Simley E, Fleming P, King J. Design and analysis of a wake steering controller with wind direction variability. Wind Energy Sci 2020;5:451–68. https://doi.org/10.5194/wes-5-451-2020.

[14] Rott A, Doekemeijer B, Kristina Seifert J, Van Wingerden JW, Kühn M. Robust active wake control in consideration of wind direction variability and uncertainty. Wind Energy Sci 2018;3:869–82. https://doi.org/10.5194/wes-3-869-2018.

[15] Quick J, Annoni J, King R, Dykes K, Fleming P, Ning A. Optimization under Uncertainty for Wake Steering Strategies. J Phys Conf Ser 2017;854. https://doi.org/10.1088/1742-6596/854/1/012036.

[16] Paul A. Fleming1, Andrew Ning1 PMOG and KD 1. Wind plant system engineering through optimization of layout and yaw control. Wind Energy 2013:1–20. https://doi.org/10.1002/we.

[17] Ke S, Wang T, Ge Y, Wang H. Wind-induced fatigue of large HAWT coupled tower–blade structures considering aeroelastic and yaw effects. Struct Des Tall Spec Build 2018;27:1–14. https://doi.org/10.1002/tal.1467.

[18] Paul Fleming1, Pieter M.O. Gebraad2, Sang Lee1, Jan-Willem van Wingerden2, Kathryn Johnson1, Matt Churchfield1, John Michalakes1 PS and PM. Simulation comparison of wake mitigation control strategies for a two-turbine case. Wind Energy 2013:1–20. https://doi.org/10.1002/we.

[19] Boorsma K, Schepers JG. New MEXICO experiment: preliminary overview with initial validation. ECN; 2014.

[20] Boorsma K. Power and loads for wind turbines in yawed conditions 2012.

[21] Ennis BL, White JR, Paquette JA. Wind turbine blade load

characterization under yaw offset at the SWiFT facility. J Phys Conf Ser 2018;1037. https://doi.org/10.1088/1742-6596/1037/5/052001.

[22] Kanev SK, Savenije FJ. Active Wake Control : loads trends. Tech Report, ECN-E--15-004 2015.

[23] Mendez Reyes H, Kanev S, Doekemeijer B, van Wingerden J-W. Validation of a lookup-table approach to modeling turbine fatigue loads in wind farms under active wake control. Wind Energy Sci 2019;4:1–19. https://doi.org/10.5194/wes-2019-34.

[24] Hansen KAK and MH. Load alleviation of wind turbines by yaw misalignment. Wind Energy 2013:1–20. https://doi.org/10.1002/we.

[25] Jasa J, Bortolotti P, Zalkind D, Barter G. Effectively using multifidelity optimization for wind turbine design 2021:1–22.

[26] Obdam TS, Braam H. Flight Leader Concept for Wind Farm Load Counting : First offshore implementation 2009:13.

[27] Cosack N, Kühn M. An approach for fatigue load monitoring without load measurement devices. Eur Wind Energy Conf Exhib 2009, EWEC 2009 2009;1:513–22.

[28] Vera-Tudela L, Kühn M. Analysing wind turbine fatigue load prediction: The impact of wind farm flow conditions. Renew Energy 2017;107:352–60. https://doi.org/10.1016/j.renene.2017.01.065.

[29] Dervilis N, Choi M, Antoniadou I, Farinholt KM, Taylor SG, Barthorpe RJ, et al. Machine learning applications for a wind turbine blade under continuous fatigue loading. Key Eng Mater 2014;588:166–74. https://doi.org/10.4028/www.scientific.net/KEM.588.166.

[30] Luna J, Falkenberg O, Gros S, Schild A. Wind turbine fatigue reduction based on economic-tracking NMPC with direct ANN fatigue

estimation. Renew Energy 2020;147:1632–41. https://doi.org/10.1016/j.renene.2019.09.092.

[31] van Dijk MT, van Wingerden JW, Ashuri T, Li Y. Wind farm multi-objective wake redirection for optimizing power production and loads. Energy 2017;121:561–9. https://doi.org/10.1016/j.energy.2017.01.051.

[32] Jonkman BJ, Kilcher L. TurbSim User's Guide. Natl Renew Energy Lab 2012:1–87.

[33] Infrastructure N, Centre SC, Infrastructure N, Reference D, Great Britain. Centre for the Protection of National Infrastructure, Murray-webster R, et al. IEC International Standard 61400-1 2005;2005:88.

[34] He R, Yang H, Sun H, Gao X. A novel three-dimensional wake model based on anisotropic Gaussian distribution for wind turbine wakes. Appl Energy 2021;296:117059.

[35] Madsen HA, Larsen GC, Larsen TJ, Troldborg N, Mikkelsen R. Calibration and validation of the dynamic wake meandering model for implementation in an aeroelastic code. J Sol Energy Eng Trans ASME 2010;132:1–14. https://doi.org/10.1115/1.4002555.

[36] Hao Y, Lackner MA, Keck RE, Lee S, Churchfield MJ, Moriarty P. Implementing the dynamic wake meandering model in the NWTC design codes. 32nd ASME Wind Energy Symp 2014:1–19. https://doi.org/10.2514/6.2014-1089.

[37] J. Jonkman, S. Butterfield, W. Musial and GS. Definition of a 5-MW Reference Wind Turbine for Offshore System Development. J Offshore Mech Arct Eng 2018;140. https://doi.org/10.1115/1.4038580.

[38] Yang Y, Bashir M, Wang J, Yu J, Li C. Performance evaluation of an integrated floating energy system based on coupled analysis. Energy Convers Manag 2020;223:113308. https://doi.org/10.1016/j.enconman.2020.113308.

[39] Yang Y, Bashir M, Michailides C, Li C, Wang J. Development and application of an aero-hydro-servo-elastic coupling framework for analysis of floating offshore wind turbines. Renew Energy 2020;161:606–25. https://doi.org/10.1016/j.renene.2020.07.134.

[40] Clark CE, Barter G, Shaler K, DuPont B. Reliability-based layout optimization in offshore wind energy systems. Wind Energy 2021:1–24. https://doi.org/10.1002/we.2664.

[41] Jonkman JM. Modeling of the UAE Wind Turbine for Refinement of FAST _ AD Modeling of the UAE Wind Turbine for Refinement of. Contract 2003.

[42] Jonkman J, Shaler K. FAST . Farm User ' s Guide and Theory Manual 2020.

[43] Wu K, Zhou H, An S, Huang T. Optimal coordinate operation control for wind-photovoltaic-battery storage power-generation units. Energy Convers Manag 2015;90:466–75. https://doi.org/10.1016/j.enconman.2014.11.038.

[44] Miner MA. Cumulative damage in fatigue 1945.

[45] Wang Y, Miao W, Ding Q, Li C, Xiang B. Numerical investigations on control strategies of wake deviation for large wind turbines in an offshore wind farm. Energy Convers Manag 2019;173:794–801. https://doi.org/10.1016/j.oceaneng.2019.01.042.

[46] Shamshirband S, Petković D, Amini A, Anuar NB, Nikolić V, Ćojbašić Ž, et al. Support vector regression methodology for wind turbine reaction torque prediction with power-split hydrostatic continuous variable transmission. Energy 2014;67:623–30. https://doi.org/10.1016/j.energy.2014.01.111.

[47] Santamaría-Bonfil G, Reyes-Ballesteros A, Gershenson C. Wind

speed forecasting for wind farms: A method based on support vector regression. Renew Energy 2016;85:790–809. https://doi.org/10.1016/j.renene.2015.07.004.

[48] Khosravi A, Koury RNN, Machado L, Pabon JJG. Prediction of wind speed and wind direction using artificial neural network, support vector regression and adaptive neuro-fuzzy inference system. Sustain Energy Technol Assessments 2018;25:146–60. https://doi.org/10.1016/j.seta.2018.01.001.

[49] Ti Z, Deng XW, Yang H. Wake modeling of wind turbines using machine learning. Appl Energy 2020;257:114025. https://doi.org/10.1016/j.apenergy.2019.114025.

[50] Drucker H, Burges CJC, Kaufman L, Smola A, Vapnik V. Support vector regression machines. Adv Neural Inf Process Syst 1997;9:155–61.

[51] Fleming PA, Gebraad PMO, Lee S, van Wingerden JW, Johnson K, Churchfield M, et al. Evaluating techniques for redirecting turbine wakes using SOWFA. Renew Energy 2014;70:211–8. https://doi.org/10.1016/j.renene.2014.02.015.

[52] Bastankhah M, Porte-Agel F. Wind tunnel study of the wind turbine interaction with a boundary-layer flow: Upwind region, turbine performance, and wake region. Phys Fluids 2017;29. https://doi.org/10.1063/1.4984078.

[53] Choi D, Shin W, Ko K, Rhee W. Static and Dynamic Yaw Misalignments of Wind Turbines and Machine Learning Based Correction Methods Using LiDAR Data. IEEE Trans Sustain Energy 2019;10:971–82. https://doi.org/10.1109/TSTE.2018.2856919.